Baryon Number Correlations in Heavy Ion Collisions

Apoorva Patel[*]

Centre for High Energy Physics and
Supercomputer Education and Research Centre,
Indian Institute of Science, Bangalore 560012, India
E-mail: `adpatel@cts.iisc.ernet.in`

The cross-over region of the quark-gluon plasma (QGP) created in heavy ion collisions is influenced by the nearby deconfinement, chiral and baryon condensation phase transitions. A characteristic signature of the deconfinement transition in this region can be inferred using the flux tube model, which is dual to the Polyakov loop description and which offers a visual picture of what happens during the transition. The three-point (anti)vertices of a flux tube network lead to formation of (anti)baryons upon hadronisation. Since there is no fundamental interaction associated with the baryon number, correlations in the baryon number distribution at the last scattering surface directly reflect the preceding pattern of the flux tube vertices in the QGP. An alternating pattern of vertices and antivertices would lead to an oscillatory signal in the two-point baryon number correlations, under the experimental conditions prevalent in heavy ion collisions at RHIC and LHC. The strength of the oscillations is a measure of the flexibility of the QGP.

---

[*]Speaker.

The study of collective non-perturbative phenomena in QCD at high temperatures and/or at large chemical potentials is a highly active area of research: experimentally through heavy ion collisions [1], theoretically through phenomenological models [2], and computationally through lattice QCD simulations [3]. Consider QCD with $N = 3$ colours and N_f degenerate quark flavours of mass m, at temperature T and quark chemical potential μ. The phase structure of this theory is depicted in Fig.1(a) in a schematic manner. Three corners of the phase structure are well-understood because of the exact symmetries present there: (a) the finite temperature deconfinement phase transition at $m = \infty$, governed by the global Z_3 centre symmetry of the Polyakov loop, (b) the finite temperature chiral phase transition at $m = 0 = \mu$, governed by the flavour $SU(N_f)_L \otimes SU(N_f)_R$ symmetry, and (c) the baryon condensation phase transition at $m = 0 = T$, when μ crosses the constituent quark mass. These end-points are first-order phase transitions, and phase transition surfaces extend inwards from them. Phenomenological and numerical studies show that the surfaces end in critical lines, and there is no phase transition for the physical values of the quark masses as T is varied (unless μ is sufficiently large). Nevertheless, the three nearby transitions cause various QCD properties to change rapidly in the cross-over region. To enhance our understanding of QCD, it is important to construct observables that can be extracted from the experimental data and that can highlight the dynamical features of deconfinement, chiral symmetry restoration and baryon condensation.

In this article, I describe how the deconfinement phase transition leaves a signature in two-point baryon number correlations in the angular distribution of the hadrons produced in heavy ion collisions. The collisions at RHIC and LHC create a high energy state of QCD matter, which upon cooling produces $O(1000)$ hadrons. These hadrons are dominated by pions, but also include $O(100)$ baryons and antibaryons. The particle numbers are large enough for one to analyse their distributions in position, momenta and energy (instead of only looking at individual particle properties). For the statistical distributions to be meaningful, they have to arise from some reasonably
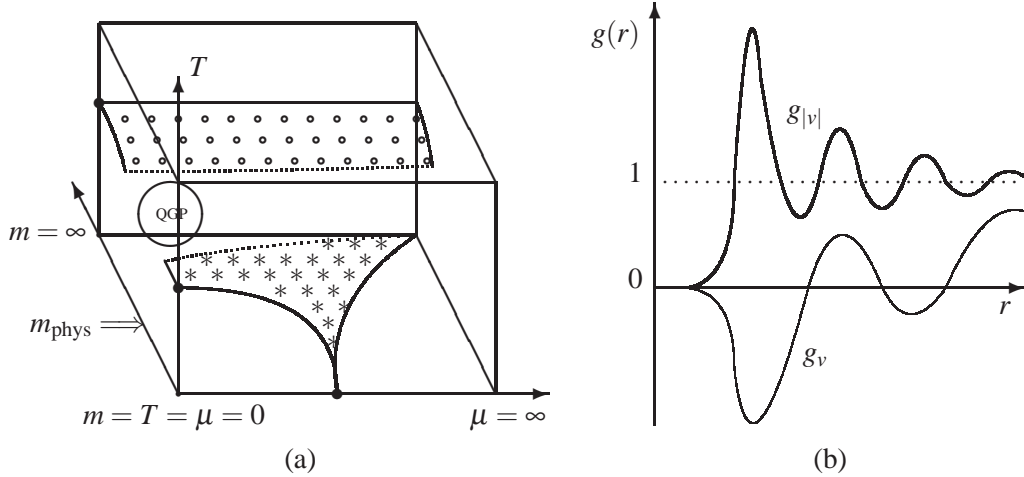

(a)   (b)

Figure 1: (a) Schematic description of the QCD phase structure in the $m - T - \mu$ space. The first-order transition surfaces are shown shaded, and the critical lines are shown dotted. The value of m corresponding to the real world QCD, and the QGP region accessible in heavy-ion collisions, are pointed out.
(b) Schematic representation of the anticipated baryon number two-point correlation functions, $g_{|v|}(r)$ (thick line) and $g_v(r)$ (thin line). The former is similar to that for objects with hard-core repulsion. The latter is for a percolating flux tube network where vertices and antivertices alternate.

equilibrated state. Experimental data suggest that such an approximately thermalised quark-gluon plasma (QGP) is created, with energy density $\varepsilon \simeq 1\text{GeV}/\text{fm}^3$ and temperature $T_{\text{cr}} \simeq 175\text{MeV}$, in the fireball of central collisions and produces moderate p_T hadrons. An important limitation of the experiments is that they detect only charged hadrons moving in sufficiently transverse directions.

The experimentally observed multiplicities and distributions of various particles have been fitted to hadron resonance gas models, resulting in estimates of the "chemical freeze-out" temperature (where inelastic scattering stops) and the "kinetic freeze-out" temperature (where elastic scattering stops) [4]. The stage is now set to go beyond the average properties and investigate the two-point correlations in the distributions. A useful analogy is the study of the cosmic microwave background radiation (CMBR), where first the black body spectrum was determined, and then temperature fluctuations were detected at the level of $\Delta T \simeq 10^{-5}T$ with characteristic angular correlations [5]. The "last scattering surface" in the evolution of the CMBR is analogous to the "kinetic freeze-out" stage of the QCD fireball. The patterns that can be observed there would be an invaluable help in understanding the QGP dynamics that preceded it.

In what follows, I first present a flux tube model providing a physical picture of the deconfinement process [6], and then point out that under suitable conditions the scenario predicts a specific two-point baryon number correlation signal [7], illustrated in Fig.1(b). The challenge for theorists is to quantify this signal as much as possible, and the challenge for experimentalists is to detect it.

1. Flux Tube Model Phenomenology

The flux tube model of QCD is motivated by the dual superconductor description of linear colour confinement [8], where condensation of colour magnetic charges restricts colour electric fields to vortex-like configurations. The model is phenomenologically quite successful, and is manifest in lattice QCD results as the area law for large Wilson loops. A characteristic property of the flux tube is its energy per unit length, i.e. the string tension σ. Other than that, the flux tube has a finite width w and a persistence length a, both of order Λ_{QCD}^{-1}.

The flux tubes have to obey the constraint of Gauss's law. So they terminate only on quarks, and interact only at 3-point vertices. These two features represent the invariant tensors δ_{ab} and ε_{abc} used to describe the meson and the baryon wavefunctions, and are illustrated by the lattice QCD simulation results displayed in Fig.2. Other multi-quark hadron states are phenomenologically not prominent, and so all other interactions among the flux tubes are ignored in the model.
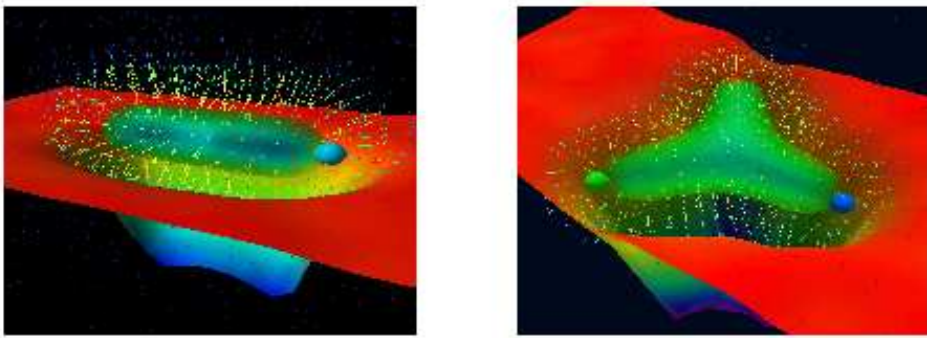

Figure 2: Gluon flux tube configurations between static (anti)quark sources determined by lattice QCD simulations [9]. A meson is on the left and a baryon is on the right.

The finite temperature behavior of the model is governed by competition between the energy and the entropy of the flux tube configurations. At low temperatures, energy wins, keeping down the total length of the flux tubes. At high temperatures, entropy dominates, producing elaborate structures of the flux tubes all over the space. As the temperature is increased the flux tubes oscillate more, and also produce more vertices. Some of the possible configurations are shown in Fig.3(a)-(d). First consider the pure gauge theory, i.e. $m = \infty$. In absence of vertices, there is a second-order deconfinement phase transition, where the flux tube length diverges and the quark-antiquark pair loses information about each-other's position. In presence of vertices, the flux tubes can percolate the space in a network before the correlation length diverges. That also allows the quark-antiquark pair (hooked on to the network) to lose information about each-other's position, but produces a first-order deconfinement phase transition.

When finite mass quarks are included in the model, they break the flux tubes by quark-antiquark pair production from the vacuum. With the flux tube network breaking up, the deconfinement phase transition weakens as the quark mass is lowered from $m = \infty$ and/or as the chemical potential is increased. Numerical estimates show that for $N_f = 3$ QCD at small chemical potentials, the first-order deconfinement phase transition ends in a critical line around $m = 1.5\text{GeV}$, as depicted in Fig.1(a). Although the cross-over region does not have any sharp signal of the deconfinement phase transition, the percolating flux tube scenario still suggests a detectable observable there.

It is straightforward to formulate the model on a lattice with spacing a. The flux tubes live on the links, while the quarks and vertices live on the sites. The variables take values $0, \pm 1$, depending on the direction of the flux, as shown in Fig.3(e). The total energy of a flux tube configuration is

$$E = \sigma a \sum_{i,\mu} |n_{i,\mu}| + m \sum_{i,f} |p_{i,f}| + v \sum_i |q_i| , \qquad (1.1)$$

where v denotes the energy cost of a vertex, and f sums over the $2N_f$ spin and flavour quark degrees of freedom. The constraint of Gauss's law at every site is

$$\sum_{\mu} (n_{i,\mu} - n_{i-\mu,\mu}) - \sum_f p_{i,f} + 3q_i \equiv \alpha_i = 0 . \qquad (1.2)$$
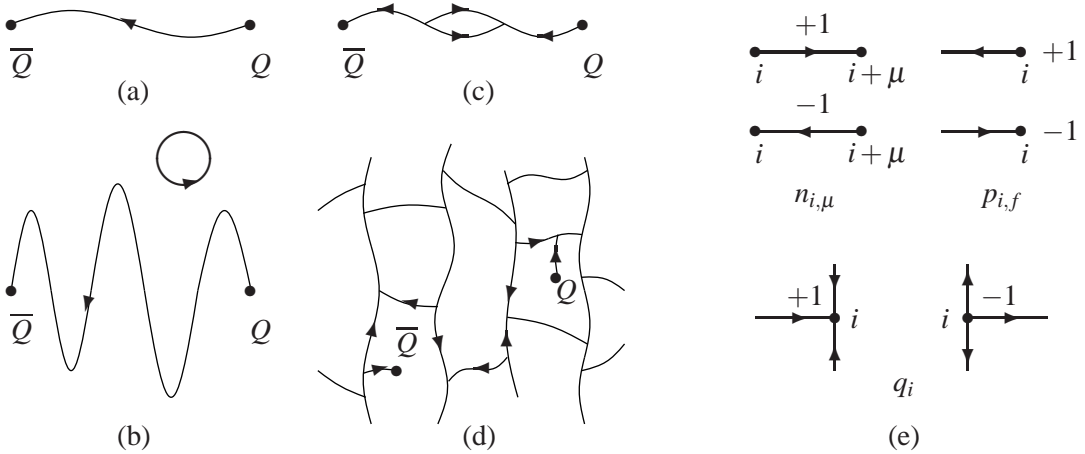

Figure 3: (a)-(d) depict possible flux tube configurations connecting a static quark-antiquark pair. Increasing temperature takes (a) to (b) and (c) to (d), while creation of baryonic vertices takes (a) to (c) and (b) to (d). (e) lists the link and the site variables used for formulating the flux tube model on a lattice.

The grand canonical partition function for the system, with baryon number B, is

$$Z[T,\mu] = \sum_{n_{i,\mu},\, p_{i,f},\, q_i} \exp\left[-\frac{E-3\mu B}{T}\right] \prod_i \delta_{\alpha_i,0} \,, \quad B = \frac{1}{3}\sum_{i,f} p_{i,f} = \sum_i q_i \,. \qquad (1.3)$$

It is fully factorised by expressing the constraint at every site as $\delta_{\alpha_i,0} = \int_{-\pi}^{\pi}(d\theta_i/2\pi)e^{i\alpha_i\theta_i}$. The sum over the variables $n_{i,\mu}$, $p_{i,f}$, q_i can then be carried out explicitly, resulting in

$$Z[T,\mu] = \int_{-\pi}^{\pi} \prod_i \frac{d\theta_i}{2\pi} \prod_{i,\mu}(1+2e^{-\sigma a/T}\cos(\theta_{i+\mu}-\theta_i))$$

$$\times \prod_i \left(1+2e^{-m/T}\cos\left(\theta_i+i\frac{\mu}{T}\right)\right)^{2N_f} \times \prod_i(1+2e^{-v/T}\cos(3\theta_i)) \,. \qquad (1.4)$$

This is in the universality class of the 3-dim XY spin model, in the presence of an ordinary magnetic field as well as a Z_3 symmetric magnetic field. In this form, $Z[T,\mu]$ possesses a generalised $\mathscr{PT}$ symmetry, with $\mathscr{P}$ corresponding to $\theta_i \to -\theta_i$ and $\mathscr{T}$ corresponding to complex conjugation. As a consequence, even though Eq.(1.4) involves complex weights, the equivalent form in Eq.(1.3) can be numerically simulated without any fermion sign problem at finite chemical potential [10, 11].

Physical interpretation of the site variables θ_i is uncovered by insertion of static sources in the system. A static quark at site j modifies the Gauss's law constraint there as $\delta_{\alpha_j,0} \to \delta_{\alpha_j,-1}$, and its free energy is given by $\exp(-F_q/T) = \langle\exp(-i\theta_j)\rangle$. In the gauge field theory language, this quantity is the expectation value $\langle P_j\rangle$ of the Polyakov loop at site j. So we infer that θ_j represents the phase of the Polyakov loop P_j, and the flux tube description of deconfinement is dual to the familiar Polyakov loop description of deconfinement. The benefit of the flux tube description is the visual representation it provides of what happens in position space as the temperature is varied.

2. Predicted Signal in Heavy Ion Collisions

Let us consider the flux tube scenario as the fireball of QGP in heavy ion experiments expands and cools. The cross-over region does not possess a single percolating flux tube network, but it can still contain many finite clusters of flux tubes. Since the flux is directed, an obvious feature of every cluster is that any neighbour of a vertex is an antivertex and vice versa (see Fig.3(d)). This is a topological feature, rather immune to the details of QCD dynamics. Conservation of baryon number implies that the vertices can only be locally pair-produced or pair-annihilated. As the QGP hadronises, the flux tube clusters start breaking up. After the chemical freeze-out stage, there is no more production or annihilation of vertices; every vertex ends up in a baryon and every antivertex ends up in an antibaryon. In the absence of subsequent large-scale diffusion, the radial propagation of (anti)baryons preserves the geometric pattern of (anti)vertices present at the chemical freeze-out stage, and the angular positions of the (anti)baryons seen in the detector can be backtracked to the angular positions of the (anti)vertices at the chemical freeze-out stage. This pattern of vertices can then be analysed for correlations and fluctuations, using techniques similar to those used to analyse the temperature correlations and fluctuations in the CMBR [5].

Numerical simulations can calculate the equilibrium correlations between flux tube vertices in the 3-dim position space, which can then be projected onto the observed surface of the fireball.

Flux tube clusters are bipartite graphs of degree 3. Their alternating neighbour pattern of vertices and antivertices can yield two-point baryon number correlations similar to the oscillatory two-point charge correlations in ionic liquids, illustrated in Fig.1(b). The key common ingredient in the two cases is the hard-core repulsion between the objects involved.

An oscillatory behaviour of the two-point baryon number correlations requires the following (in a mimicry of the Sakharov conditions): (1) A mechanism for local baryon-antibaryon pair production must exist. This is inherent in the QCD dynamics. (2) The system must have a non-zero chemical potential (analogous to a Fermi surface in condensed matter systems). This avoids spectral positivity constraints, as in case of $\mathscr{PT}$ symmetric systems [11], and is true in experiments. (3) The dynamical evolution must not be in equilibrium. This favours fragmentation of flux tube clusters during hadronisation while suppressing vertex-antivertex annihilation. Production of a sizeable number of antibaryons in experiments [1], from an initial state that has none, confirms it.

For concreteness, consider a homogeneous and isotropic fluid consisting of discrete objects with charges $q_i = \pm 1$ at positions r_i. Then the average density ρ_q is independent of the position and the average two-point correlation function $g_q(\vec{r}_i, \vec{r}_j)$ depends only on $r = |\vec{r}_i - \vec{r}_j|$:

$$\rho_q = \left\langle \sum_i q_i \, \delta(\vec{r}_i) \right\rangle, \qquad \rho_q \, g_q(r) = \left\langle \sum_{i \neq 0} q_i \, \delta(r - |\vec{r}_i - \vec{r}_0|) \right\rangle. \tag{2.1}$$

Interactions fade away at long distances, and so $g(r \to \infty) = 1$. For objects with hard-core repulsion, $g(0) = 0$, and beyond the hard core $g(r)$ tends to its asymptotic value exhibiting damped oscillations [12]. In particular, the distance scale of the oscillations is determined by the inter-object separation, and the amplitude of the oscillations is determined by how tightly the objects are packed together.

To quantify the correlation between vertices and antivertices, it is useful to compare the correlation functions g_v and $g_{|v|}$ on the same data sets, respectively obtained with and without the factors of q_i in Eq.(2.1). They are sketched in Fig.1(b), and their comparison reduces systematic effects arising from varying fireball sizes. $g_{|v|}(r)$ is rather insensitive to interactions other than the hard core. Its first peak is the most informative one regarding the equilibrium fluid properties—with the location, the height and the area under it respectively giving estimates of the inter-object spacing, the fluid compressibility and the number of nearest neighbours. On the contrary, successive correlated neighbours contribute with opposite signs to $g_v(r)$. For a system with no correlations between vertices, the probability of occurrence of a vertex or an antivertex at any location is proportional to its overall density, and $g_v(r)$ behaves the same way as $g_{|v|}(r)$. Thus the contrast between $g_v(r)$ and $g_{|v|}(r)$, which is maximum at the first peak, is a measure of the vertex-antivertex correlations.

Note that a break-up of the flux tube clusters smoothens the oscillations of the two-point correlation functions, similar to what happens when a fluid is warmed. Still, if large enough flux tube clusters remain in the QGP, they would contribute to the contrast between $g_v(r)$ and $g_{|v|}(r)$. So the strength of the contrast measures the extent to which the nearby deconfinement phase transition influences QGP properties in the cross-over region. Specifically, the features to be quantified are the distance scale and the amplitude of the oscillatory signal. The former is expected to be the inter-baryon separation (~ 2 fm), while the latter indicates how tightly or softly the QGP is packed.

Projection of the 3-dim correlation functions onto the observed surface of the fireball smears their oscillatory structure. That is an easily calculable effect as long as the inter-vertex separation is smaller than the radius of the fireball [7]. More importantly, the angular coverage of the ex-

perimentally observed hadron distributions is limited. A partial Fourier expansion, based on the rotation symmetry around the beam axis and parity, helps in the search for correlations by orthogonal separation of scales. Labeling the angular distributions by the unit vector $\hat{n}(\theta,\phi)$, we have

$$b(\hat{n}) = \frac{1}{\sqrt{2\pi}} \sum_{\sigma=\pm} \sum_{m=-\infty}^{\infty} b_m^\sigma(\theta)\, e^{im\phi} \ , \quad \langle b(\hat{n}) b(\hat{n}') \rangle = \frac{1}{2\pi} \sum_{\sigma=\pm} \sum_{m=-\infty}^{\infty} C_m^\sigma(\theta,\theta')\, e^{im(\phi-\phi')} \ . \quad (2.2)$$

These expansions of baryon number distributions can be inverted as

$$C_m^\sigma(\theta,\theta') = \frac{1}{2\pi} \int_0^{2\pi} d\phi \int_0^{2\pi} d\phi'\, e^{im(\phi'-\phi)} \langle b^\sigma(\hat{n}) b^\sigma(\hat{n}') \rangle \ , \quad b^\pm(\hat{n}) = \frac{1}{2} \left(b(\hat{n}) \pm b(-\hat{n}) \right) \ . \quad (2.3)$$

The real and symmetric coefficient functions $C_m^\pm(\theta,\theta')$ contain all the information about the two-point correlation functions, and their experimental values can be tested against model predictions.

The biggest gap between the theoretical formalism and the experimental data is the fact that the detectors observe protons and anti-protons but miss neutrons and anti-neutrons. One has to rely on the isospin symmetry to assume that the observed subset of (anti)protons provides a faithful characterisation of the total baryon number distribution. Corrections also need to be estimated for only approximate equilibration of the fireball, non-uniformity of the QGP caused by the elliptic flow, baryon number diffusion subsequent to hadronisation and development of the hard baryon core during hadronisation. Nevertheless, it is imperative to extract the two-point baryon number correlations from the experimental data and compare them to theoretical estimates. That would tell us a lot about where exactly the QGP lies between the extremes of a rigid crystal and a dilute gas.

References

[1] See for instance, B. Abelev *et al.* (STAR Collaboration), *Phys. Rev.* **C 79** (2009) 034909; C. Loizides, in proceedings of *23rd Rencontres de Blois, Particle Physics and Cosmology*, `http://lss.fnal.gov/conf2/C110529/loizides.pdf` (2011).

[2] See for instance, D. Kharzeev, *Nucl. Phys.* **A 827** (2009) 118c; L. McLerran, *Nucl. Phys.* **A 862-863** (2011) 251.

[3] See for instance, S. Gupta, `PoS(Lattice 2010)007`; K. Kanaya, `PoS(Lattice 2010)012`.

[4] U.W. Heinz, in proceedings of *2003 CERN-CLAF School of High-Energy Physics*, ed. N. Ellis (CERN, Geneva, 2006), p.165 [`hep-ph/0407360`].

[5] S. Weinberg, *Cosmology*, Oxford University Press, New York, 2008.

[6] A. Patel, *Nucl. Phys.* **B 243** (1984) 411; *Phys. Lett.* **139B** (1984) 394.

[7] A. Patel, *Phys. Rev.* **D 85** (2012) 114019.

[8] G. Ripka, *Dual Superconductor Models of Color Confinement*, Lecture Notes in Physics, Vol. 639, Springer, Berlin, 2004.

[9] F. Bissey, F.G. Cao, A.R. Kitson, A.I Signal, D.B. Leinweber, B.G. Lassock and A.G.Williams, *Phys. Rev.* **D 76** (2007) 114512.

[10] Y.D. Mercado, H.G. Evertz and C. Gattringer, *Phys. Rev. Lett.* **106** (2011) 222001.

[11] M.C. Ogilvie, P.N. Meisinger and T.D. Wiser, *Int. J. Theor. Phys.* **50** (2011) 1042.

[12] P.M. Chaikin and T.C. Lubensky, *Principles of Condensed Matter Physics*, Cambridge University Press, Cambridge, 2000.